

Tension-induced non-linearities of flexural modes in nanomechanical resonators

Raphaël Khan,^{1,*} F. Massel,¹ and T. T. Heikkilä¹

¹*Low Temperature Laboratory, Aalto University, P.O. Box 15100, FI-00076 AALTO, Finland*

(Dated: July 28, 2021)

We consider the tension-induced non-linearities of mechanical resonators, and derive the Hamiltonian of the flexural modes up to the fourth order in the position operators. This tension can be controlled by a nearby gate voltage. We focus on systems which allow large deformations $u(x) \gg h$ compared to the thickness h of the resonator and show that in this case the third-order coupling can become non-zero due to the induced dc deformation and offers the possibility to realize radiation-pressure-type equations of motion encountered in optomechanics. The fourth-order coupling is relevant especially for relatively low voltages. It can be detected by accessing the Duffing regime, and by measuring frequency shifts due to mode-mode coupling.

PACS numbers: 85.85.+j

Recent progress in fabricating nanomechanical resonators has shown how these systems can be used for ultrasensitive measurements of mass, force and charge [1–4]. Within the couple of past years these systems have also entered the quantum realm [5] as superpositions of vibration states and zero-point vibrations have been measured. Even though such measurements can be performed in a regime where the elastic properties of the resonators could essentially be considered as linear, the extension to non-linear conditions is well within reach of the current experimental techniques.

In this paper we consider the generic non-linearities of the resonators, how these show up in measurements, and how they arise when the resonators are manipulated electronically. In general, the effect of non-linearities is twofold: on one hand they modify in an amplitude-dependent way the resonant frequency of a given normal mode (Duffing self-non-linearity); on the other, they introduce a coupling between normal modes. Such non-linearities show up in the presence of strong external driving, which allows to control the coupling of different modes or to detect their occupation numbers.

Motivated by the recent advances in fabricating graphene and carbon nanotube resonators [4, 6], we concentrate especially on the regime of thin resonators where the mechanical deformation can be large compared to the resonator thickness. In this case, the major source of non-linearity is the tension induced by the deformation itself. Starting from the mechanical energy of the deformations, we derive the generic Hamiltonian of the flexural modes, including non-linearities up to the fourth order in the vibration amplitudes. In contrast to the results discussed in Refs. [7, 8], where it is not taken into account, we explicitly consider the dc deformation of the resonator. This additional aspect creates an asymmetry in our system which leads to a cubic non-linearity. The dc deformation, dictating the strength of the non-linearity, is driven by a nearby gate voltage as in Fig. 1. Concentrating first on the Duffing self-non-linearity of the modes, this then allows us to derive the voltage depen-

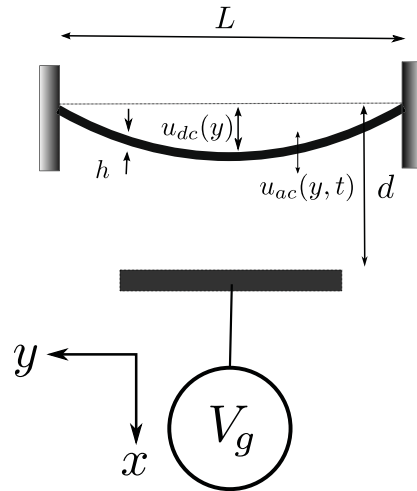


FIG. 1. Schematic picture of the studied setup : a metallic beam whose deformation is controlled by a gate voltage V_g coupled to the beam via capacitance $C(d - u(x, t))$.

dence of the Duffing constant and show that it changes sign for a certain value of voltage that depends on mode index and the amount of initial tension. This sign change results primarily from the cubic non-linearity. Therefore, studies of the Duffing constant reveal information about the parameters of the system, in particular on the initial tension, which may otherwise be difficult to obtain by only concentrating on the voltage dependence of the mode eigenfrequencies. We go on to analyze the inter-mode coupling and show that the non-linearities allow creating a radiation-pressure-type coupling between the different flexural modes. Such a coupling allows realizing optomechanics-type experiments, where one of the modes is cooled or heated by driving another mode. We provide quantitative predictions for the optical spring effect (driving-induced frequency shift) and changes in effective mode damping responsible for the cooling/heating behavior and show how these can be tuned by the dc gate voltage. The general Hamiltonian describing a non-linear

resonator is of the form

$$H = \sum_n \omega_n \hat{a}_n^\dagger \hat{a}_n + \sum_{nml} \mathbb{T}_{nml} \hat{x}_n \hat{x}_m \hat{x}_l + \sum_{nmlk} \mathbb{F}_{nmlk} \hat{x}_n \hat{x}_m \hat{x}_l \hat{x}_k + O(\hat{x}_o \hat{x}_n \hat{x}_m \hat{x}_l \hat{x}_k). \quad (1)$$

Here $\hat{x}_n = a_n^\dagger + a_n$ are the dimensionless position operators. The non-linearities are described by the coefficients \mathbb{T}_{nml} and \mathbb{F}_{nmlk} . The presence of \mathbb{T}_{nml} , like any odd non-linearities, arises from an asymmetry in the system. In the following we consider a mechanical resonator exhibiting the non-linearities discussed above. We analyse a beam of mass m with length L , thickness h and cross-section S suspended on top of a gate capacitor at voltage V_g (see Fig. 1). The flexural vibrations are characterized by the deformation $u(x, t)$ of the beam. Defining $z = y/L$, $u' = \partial_z u$ and introducing the notation $\langle u|v \rangle = \int_0^1 u(z, t) \cdot v(z, t) dz$ one can obtain (1) from the elastic energy of a resonator [9]

$$\begin{aligned} \varepsilon[u(x, t)] = & \underbrace{\frac{EI_y}{2L^3} \langle u''|u'' \rangle}_{\frac{1}{2} m \omega_s^2} + \underbrace{\frac{T_0}{2L} \langle u'|u' \rangle}_{\frac{1}{2} \tau_0 m \omega_s^2} \\ & + \underbrace{\frac{ES}{8L^3} \langle u'|u' \rangle^2}_{\frac{1}{2h^2} m \omega_s^2} + \varepsilon_{\text{force}}[u(x, t)], \quad (2) \end{aligned}$$

with E the Young modulus, I_y the bending moment, T_0 the initial tension of the resonator and $\varepsilon_{\text{force}}$ the potential energy of the force acting on the resonator. The latter is of the form $\varepsilon_{\text{force}} = -(V_g^2/2) \int_0^1 C[d - u(z, t)] dz$, where $C[d]$ is the capacitance between the gate and the beam at the distance d . In order to arrive at a Hamiltonian of the form given in Eq. (1), we assume that the gate voltage V_g is the sum of a DC part V_{dc} and a small AC part $V_{ac} \ll V_{dc}$. These voltages lead to a static deformation $u_{dc}(x) \ll d$ and a time varying part $u_{ac}(x, t) \ll u_{dc}(x)$. Expanding $u_{ac}(x, t)$ on an arbitrary basis $\chi_n(x)$, $u_{ac} = h \sum_n y^n(t) \chi_n(x)$, we can write the potential energy containing terms with two, three and four y^n s. Writing the Hamiltonian in terms of the stress energy $E_{\text{stress}} = m \omega_s^2 h^2 / 2 = ES h^4 / (8L^3)$, these terms are characterized by the dimensionless parameters which we denote by $[\Omega^2]_m^n$, Λ_{mo}^n , and Θ_{mp}^{no} for the second-, third- and fourth-order terms, respectively. These parameters are described in detail in the Appendix [10]. In particular, they depend on the dc bias voltage V_{dc} and the total tension T in the beam. As discussed below, the latter also depends on V_{dc} . The behavior of the coefficient $[\Omega^2]_m^n$ determines the voltage dependence of the eigenfrequency as described in [11, 12]. For $V_{dc} = 0$, third-order terms Λ_{mo}^n vanish because of symmetry ($u_{dc} = 0$), but for large V_{dc} they grow as $\Lambda_{mo}^n \propto V_{dc}^{2/3}$. The voltage dependence of the fourth-order terms Θ_{mp}^{no} on the other

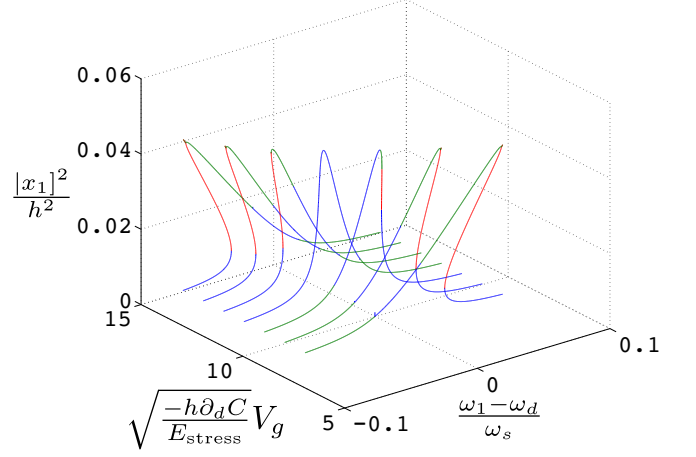


FIG. 2. (Color online) Frequency response function for the first mode with $\gamma^2 = 0.01 \omega_s^2$ and $|f_d|^2 = 0.002 m^2 \omega_s^2 h^2$. Here $E_{\text{stress}} = ES h^4 / (8L^3)$.

hand is weak and in our analytical approximations [10] disregarded altogether.

We arrive at the desired form (1) by writing the Hamiltonian in a basis which diagonalises $[\Omega^2]_m^n$ and scaling the amplitude $h y_n$ of each mode by its zero point motion $x_{zp_n} = \sqrt{\frac{1}{m \omega_n}}$ [13]. Non-linearities are coming primarily from the induced tension, which is maximized for large deformations $u(x) \gg h$. Therefore we concentrate on systems which allow large deformations, i.e., systems with $d \gg h$. We truncate the expansion to the fourth order as in the model employed above the higher-order couplings are relevant only close to the point where the beam pulls into contact with the gate plane [12].

As an example, a single-layer graphene sheet with $h = 0.34$ nm, $L = 1$ μm , $S/h = 1$ μm , $E = 1$ TPa and mass density $\rho = 1400$ kg/m³ would have $\omega_s = 250$ MHz and $E_{\text{stress}} = 0.01$ eV.

Self-non-linearity. Let us first consider the non-linear effects which occur when driving mode n with a driving force $f_d \cos(\omega_d t)$, $\omega_d \approx \omega_n$, disregarding the coupling to the other modes, as in the absence of direct driving of the other modes these would show up only in a higher order in the non-linear coupling constants. We also exclude the special case when 2 or 3 times the mode frequency matches one of the other mode frequencies [14–16]. Including dissipation the equation of motion for the amplitude x_n of mode n is

$$\ddot{x}_n + \omega_n^2 x_n + \gamma \dot{x}_n + 3\mathcal{T}_n x_n^2 + 4\mathcal{F}_n x_n^3 = \frac{f_d}{m} \cos(\omega_d t). \quad (3)$$

Here $x_n = x_{zp_n} \hat{x}_n$, $\omega_n = \omega_s (\Omega_n^n)_d$, $\mathcal{T}_n \equiv \frac{1}{2} \frac{\omega_s^2}{h} (\Lambda_{nn}^n)_d$, $\mathcal{F}_n \equiv \frac{1}{2} \frac{\omega_s^2}{h^2} (\Theta_{nn}^{nn})_d$ and the subscript d denotes that the tensors are written in the basis which diagonalises $[\Omega^2]$. The frequency response equation of (3) can be solved

from [14, 17]

$$|x_n|^2 = \frac{|f_d|^2/m^2}{\gamma^2 + \left[(\omega_n - \omega_d) - \frac{3}{8} \frac{D}{\omega_n} |x_n|^2 \right]^2}, \quad (4)$$

where γ is the damping constant and $D = 4\mathcal{F}_n - \frac{10}{8} \left(\frac{\mathcal{T}_n}{\omega_n} \right)^2 = \omega_s^2/(2h^2) [(\Theta_{nn}^{nn})_d - 5(\Lambda_{nn}^n)_d^2/[2(\Omega_n^d)^2]]$. This frequency response function is the same as one would get when considering only the fourth-order non-linearity \mathcal{F}_n , i.e, a Duffing oscillator. The effect of the third-order non-linearity \mathcal{T}_n is to shift the value of the cubic non-linearity in the frequency response function [17].

An example response function obtained for different dc gate voltages is plotted in Fig. 2 and shows up a crossover from $D > 0$ (hardening) to $D < 0$ (softening). The dc voltage dependence of D is plotted in Supplementary information [10] for a few different magnitudes of initial tension T_0 , characterized by the dimensionless quantity $\tau_0 = 4T_0L^2/(ESh^2) = h^2T_0/(2E_{\text{stress}}L)$. Here we characterize its overall behaviour. The behavior of the Duffing constant depends on the total tension T of the beam which is the sum of the initial tension T_0 and the tension induced by the deformation $u_{dc}(x)$ caused by V_{dc} . The latter has to be calculated self-consistently from the Euler–Bernoulli equation as discussed in [11]. In what follows, we describe this behavior in terms of the dimensionless quantity $\tau = 4TL^2/(ESh^2) = h^2T/(2E_{\text{stress}}L)$. In the limit $d \gg h$ it satisfies [10]

$$\begin{aligned} \tau &= \tau_0 + 2 \int_0^1 u_{dc}^2 dz \\ &= \tau_0 + \frac{\tilde{V}^4}{96\tau^2} \left(1 - \frac{3\sqrt{3}}{\sqrt{\tau}} + \frac{8}{\tau} \right), \end{aligned} \quad (5)$$

with $\tilde{V}^2 = (-h\partial_d CV_g^2)/E_{\text{stress}}$. This equation is valid provided the resultant $\tau \gtrsim 1$. In the same limit, we find for the Duffing coefficient of the fundamental mode $n = 1$

$$D = \frac{\omega_s^2}{2h^2} \left[\pi^4 - \frac{5}{8} \frac{\pi^4 f_1(\tau)^2 \tilde{V}^4}{S h^2 + \tau \pi^2 + f_1(\tau)^2 \frac{\tilde{V}^4}{8\tau^2}} \right], \quad (6)$$

where $f_n(\tau) = 2n\pi[2/(n\pi)^2 - \sqrt{3\tau}/((n\pi)^2 + 3\tau)]$ for n odd and zero otherwise. For a rectangular beam $I_y/(Sh^2) = 1/12$, but the overall behavior of D does not greatly depend on the exact shape of the beam.

Solving Eqs. (5) and (6) allows us to find the approximate behavior of the Duffing constant as the gate voltage is tuned. We find that D changes sign at a value of the gate voltage \tilde{V}^* that can be quite well fitted to the function $\tilde{V}^* \approx \sqrt{2}\tau^{3/4} + 8$ (see [10]) or

$$V_g^* \approx \frac{h^3}{2.4(-h\partial_d C)^{1/2} E_{\text{stress}}^{1/4}} T^{3/4} + 8 \frac{E_{\text{stress}}^{1/2}}{-h\partial_d C}. \quad (7)$$

Moreover, at large values of the voltage $V_g \gg V_g^*$, D (approximately) saturates to the value $D_{\text{sat}} \approx -120\omega_s^2/h^2$.

Contrary to the fundamental mode $n = 1$, the deformation induced changes in the Duffing constant of higher-order modes are rather small compared to its value for $V_g = 0$.

Non-linear mode coupling. Let us now concentrate on the non-linear coupling between the modes [7]. Unlike in Ref. [18], where the coupling between the modes is a time-dependent linear coupling, in our system the introduction of the dc deformation leads to a radiation-pressure coupling (second term in (1)). The regime investigated here is formally analogous to the setup encountered in optomechanical systems [19–22], where an external driving electromagnetic field, coupled to a resonant cavity, alters the characteristic response parameters of a mechanical resonator. More specifically, by aptly tuning the pump frequency, it is possible to alter the resonant frequency of the mechanical resonator (optical spring effect [22–24]) and its damping, thereby inducing cooling [21] or amplification [22]. Here we consider the case where one mechanical mode, say with eigenfrequency ω_m , corresponds to the cavity mode, and another one, ω_n , to the mechanical mode. We also assume that $\omega_m > 2\omega_n$. Let us discuss what happens if the system is driven with a frequency $\omega_d = \omega_m - \Delta$, $\Delta \approx \pm\omega_n$ and probed around ω_n .

Neglecting other modes, the Hamiltonian is of the form

$$\begin{aligned} H &= \omega_n \hat{a}_n^\dagger \hat{a}_n + \omega_m \hat{a}_m^\dagger \hat{a}_m + T_n \hat{x}_n^3 + T_m \hat{x}_m^3 \\ &\quad + T_{nmm} \hat{x}_n^2 \hat{x}_m + T_{nmm} \hat{x}_n \hat{x}_m^2 + F_n \hat{x}_n^4 + F_m \hat{x}_m^4 \\ &\quad + F_{nnnm} \hat{x}_n^3 \hat{x}_m + F_{nmm} \hat{x}_n^2 \hat{x}_m^2 + F_{nmm} \hat{x}_n \hat{x}_m^3, \end{aligned} \quad (8)$$

where T_{nmo} and F_{nmop} are the sum of all the permutations of indices n, m, o, p of \mathbb{T}_{nmo} and \mathbb{F}_{nmop} , respectively, and $\mathbb{T}_{nmo} = \frac{m\omega_s^2}{h} x_{zp_n} x_{zp_m} x_{zp_o} (\Lambda_{mo}^n)_d$, $\mathbb{F}_{nmol} = \frac{m\omega_s^2}{h^2} x_{zp_n} x_{zp_m} x_{zp_l} x_{zp_o} (\Theta_{ml}^{no})_d$, $T_n \equiv T_{nnn}$ and $T_m \equiv T_{mmm}$. Using the input/output formalism [25] the equations of motion for operators \hat{a}_n and \hat{a}_m are

$$\dot{\hat{a}}_n = -i \left[\left(\omega_n \hat{a}_n + 4F_n x_n^3 + 3T_n x_n^2 \right. \right. \quad (9)$$

$$\left. \left. + 4F_{nmm} \left(\hat{a}_m^\dagger \hat{a}_m + \frac{1}{2} \right) x_n \right. \right. \\ \left. \left. + 2T_{nmm} \left(\hat{a}_m^\dagger \hat{a}_m + \frac{1}{2} \right) \right] - \frac{\gamma_n}{2} \hat{a}_n + \sqrt{\gamma_n} \hat{a}_n^{in},$$

$$\dot{\hat{a}}_m = -i \left[\Delta \hat{a}_m + 12F_m \hat{a}_m (\hat{a}_m^\dagger \hat{a}_m) \right. \quad (10)$$

$$\left. \left. + 2(T_{mnn} \hat{x}_n + F_{nmm} \hat{x}_n^2) \hat{a}_m \right] - \frac{\gamma_m}{2} \hat{a}_m + \sqrt{\gamma_m} \hat{a}_m^{in}.$$

Here we have written operator a_m in a frame rotating with frequency ω_d . We linearize (10) and (11), rewriting the operators as a sum of a static α and a fluctuating part δa , $\hat{a} = \alpha + \delta \hat{a}$. Keeping terms which are of the order of $(\frac{x_{zp_n}}{h})^2$ we obtain $\alpha_n + \alpha_n^* \approx \frac{-4T_{nmm} |\alpha_m|^2}{\omega_n}$. Solving for

$\delta\hat{a}_n$ we find the frequency response function for the input signal δa_n^{in} . It is a Lorentzian function peaked at

$$\frac{\omega_{n,\text{eff}} - \omega_n}{4|\alpha_m|^2} = F_{nnmm} - 6\frac{T_n T_{nmm}}{\omega_n} \mp \frac{1}{2}\frac{T_{nmm}^2}{\omega_n} \quad (11)$$

and whose width is

$$\frac{\gamma_{n,\text{eff}} - \gamma_n}{4|\alpha_m|^2} = \pm \frac{T_{nmm}^2}{\omega_m} Q_m. \quad (12)$$

Here $Q_m = \omega_m/\gamma_m$ is the quality factor of mode m and we have assumed for simplicity the fully side-band resolved limit $\omega_n \gg \gamma_m$. We remark that the results are similar to those obtained in optomechanics, the only difference comes from the second term in the effective frequency which is proportional to the self-non-linearity. As in the case of Duffing non-linearity we consider the limit of $\tau \gtrsim 1$. We find that the effective frequency when driving mode $m = 3$ and probing mode $n = 1$ depends on the gate voltage as

$$\frac{\omega_{1,\text{eff}} - \omega_1}{9\chi\pi^4} = 8 - \frac{3f_1(\tau)^2\tilde{V}^4}{g_1(\tilde{V}, \tau)} \mp \frac{3}{2} \frac{f_1(\tau)^2\tilde{V}^4}{\sqrt{g_1(\tilde{V}, \tau)g_3(\tilde{V}, \tau)}}, \quad (13)$$

where $g_n(\tilde{V}, \tau) = \frac{4I_y(n\pi)^4}{5h^2} + \tau(n\pi)^2 + f_n(\tau)^2\frac{\tilde{V}^4}{8\tau^2}$ and $\chi = 4m\omega_s^2|\alpha_m|^2x_{zpm}^2\frac{x_{zpn}^2}{h^2}$ describes the amplitude of the pump. The effective damping changes as

$$\frac{\gamma_{1,\text{eff}} - \gamma_1}{\chi Q_3} = \pm \frac{2(3\pi)^4 f_1(\tau)^4 \frac{\tilde{V}^4}{4\tau^2}}{g_3(\tilde{V}, \tau)}. \quad (14)$$

In Fig. 3 we plot the effective frequency and the effective damping when driving mode $m = 3$ and probing its effect on mode $n = 1$. We see that both for the red- and blue-detuned pumping, i.e., $\Delta = \pm\omega_1$, the frequency shift induced by pumping, $\omega_{1,\text{eff}} - \omega_1$, [26] is positive at low gate voltages due to the fourth-order term F_{1133} in Eq. (11), changes sign upon an increasing dc gate voltage, and tends to a voltage-independent value at large voltages. The fact that the overall frequency shift is in both cases negative — in contrast to the traditional optomechanics — results from the second term in Eq. (11), which reflects the effect of the self-non-linearity T_n , and which is independent of the sign of Δ . This behavior applies only to the combination $n = 1, m = 3$. For higher-order n , the voltage-induced changes are small compared to the frequency shift at $V_{\text{dc}} = 0$. However, choosing $n = 1$ and higher m results into more complex behavior and the spring effect $\omega_{1,\text{eff}} - \omega_1$ may change sign more than once in the case of blue detuning (see [10]).

On the other hand, the change in the effective damping (inset of Fig. 3) depends on the sign of Δ . For red detuning, $\Delta = \omega_n$, $\gamma_{n,\text{eff}}$ increases as the voltage is increased, whereas for blue detuning $\gamma_{n,\text{eff}}$ decreases. For a fixed

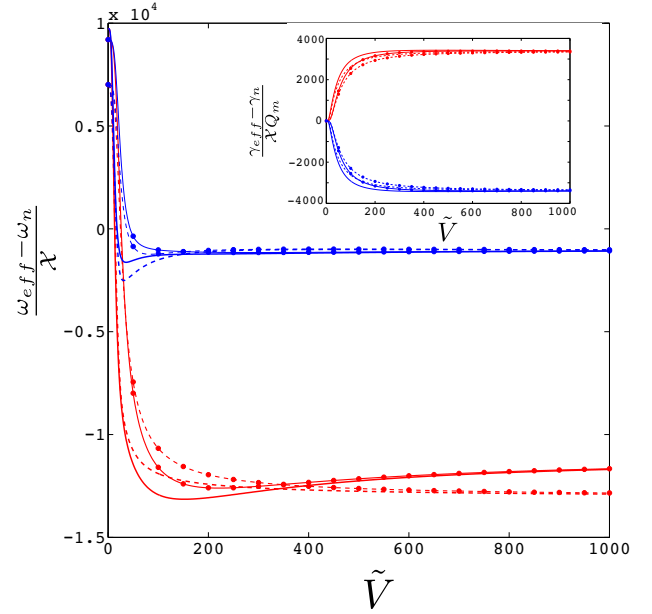


FIG. 3. (Color online) Effective frequency and damping (inset) of mode $n = 1$ when driving mode $m = 3$ with initial tension $\tau_0 = 0$ (no symbols) and $\tau = 10$ (circles) in the case of red detuning (red lines, lower) with $\Delta = \omega_1$ and in the case of blue detuning (blue lines, upper) with $\Delta = -\omega_1$. The full lines are numerical results obtained by solving the full Euler–Bernoulli equation obtained by requiring $u(x, t)$ to minimize the energy in (2), and dashed lines follow Eqs. (5), (13) and (25). Here $\chi = 4m\omega_s^2|\alpha_m|^2x_{zpm}^2\frac{x_{zpn}^2}{h^2}$ and $E_{\text{stress}} = ESh^4/(8L^3)$.

amount of fluctuations coupling to mode n , the increase in damping leads to (side-band) cooling [21], whereas the decreasing damping leads to heating and, when γ_{eff} becomes zero, to a parametric instability [27]. Between these regimes, the blue-detuned driving can be used for signal amplification [22].

In conclusion we have derived the Hamiltonian of a thin doubly clamped nanomechanical resonator taking into account the non-linearities between the amplitudes of the flexural modes induced by a nearby gate voltage. Besides the Duffing non-linearity, we also find a third order non-linearity directly related to the DC deformation of the beam. This third order non-linearity adds to the Duffing non-linearity and changes the behavior of the frequency response function. Besides the self-non-linearity described by the Duffing behavior, we find that the different modes of the beam are non-linearly coupled. The effective Hamiltonian of a pair of such modes resembles that of a mechanical degree of freedom coupled to a cavity, with the difference that in the current setup the cavity is replaced by another flexural mode. Therefore, such a coupling offers the possibility of observing the motion of one mode by observing its effect on another mode. Such effects are the spring effect and the changing damping, and the latter can be used for side-band cooling or

amplification of a given mechanical mode.

Besides the non-linearity induced by bending described here, there may be other sources of non-linearity in thin metallic beams, such as those related with non-linearities in electronic properties [28] or non-linearities induced by stretching. Our results help to identify the direct bending-induced non-linearities and therefore facilitate the precise tuning of nanomechanical resonances.

We thank Mika Sillanpää, Sung Un Cho and Xuefeng Song for useful discussions. This work is supported in part by the Academy of Finland and by the European Research Council (Grant No. 240362-Heatronics).

* raphael.khan@aalto.fi

- [1] K. Jensen, K. Kim, and A. Zettl, *Nature Nanotech.* **3**, 533 (2008)
- [2] J. Chaste, A. Eichler, J. Moser, G. Ceballos, R. Rurali, and A. Bachtold, *Nature Nanotech.* **7**, 301 (2012)
- [3] E. Gavartin, P. Verlot, and T. J. Kippenberg, *Nature Nanotech.* **7**, 509 (2012)
- [4] J. S. Bunch, A. M. v. d. Zande, S. S. Verbridge, I. W. Frank, D. M. Tanenbaum, J. M. Parpia, H. G. Craighead, and P. L. McEuen, *Science* **315**, 490 (2007)
- [5] A. D. OConnell, M. Hofheinz, M. Ansmann, R. C. Bialczak, M. Lenander, E. Lucero, M. Neeley, D. Sank, H. Wang, M. Weides, J. Wenner, J. M. Martinis, and A. N. Cleland, *Nature* **464**, 697 (2010)
- [6] A. K. Hüttel, G. A. Steele, B. Witkamp, M. Poot, L. P. Kouwenhoven, and H. S. J. van der Zant, *Nano Lett.* **9**, 2547 (2009)
- [7] H. J. R. Westra, M. Poot, H. S. J. van der Zant, and W. J. Venstra, *Phys. Rev. Lett.* **105**, 117205 (2010)
- [8] K. J. Lulla, R. B. Cousins, A. Venkatesan, M. J. Patton, A. D. Armour, C. J. Mellor, and J. R. Owers-Bradley, arXiv:1204.4487
- [9] L. D. Landau, E. M. Lifshitz, A. M. Kosevich, and L. P. Pitaevski, *Theory of elasticity* (Elsevier, 1986)
- [10] See the Appendix for details of deriving the coefficients in Eq. (3) and the details of the Duffing constant and the non-linear coupling between the modes.
- [11] S. Sapmaz, Y. M. Blanter, L. Gurevich, and H. S. J. van der Zant, *Phys. Rev. B* **67**, 235414 (2003)
- [12] M. A. Sillanpää, R. Khan, T. T. Heikkilä, and P. J. Hakonen, *Phys. Rev. B* **84**, 195433 (2011)
- [13] Even though in the following we concentrate on driving amplitudes containing many photons, and therefore deal with essentially classical non-linearities, also quantum effects related with zero-point motion could be discussed with the Hamiltonian we derive.
- [14] A. H. Nayfeh and D. T. Mook, *Nonlinear Oscillations* (John Wiley & Sons, 2008)
- [15] D. Antonio, D. H. Zanette, and D. López, *Nature Commun.* **3**, 806 (2012)
- [16] A. Eichler, M. del Álamo Ruiz, J. A. Plaza, and A. Bachtold, *Phys. Rev. Lett.* **109**, 025503 (2012)
- [17] I. Kozinsky, H. W. C. Postma, I. Bargatin, and M. L. Roukes, *App. Phys. Lett.* **88**, 253101 (2006)
- [18] I. Mahboob, K. Nishiguchi, H. Okamoto, and H. Yamaguchi, *Nat. Phys.* **8**, 387 (2012)
- [19] F. Marquardt, J. P. Chen, A. A. Clerk, and S. M. Girvin, *Phys. Rev. Lett.* **99**, 093902 (2007)
- [20] C. Genes, D. Vitali, P. Tombesi, S. Gigan, and M. Aspelmeyer, *Phys. Rev. A* **77**, 033804 (2008)
- [21] J. D. Teufel, T. Donner, D. Li, J. W. Harlow, M. S. Allman, K. Cicak, A. J. Sirois, J. D. Whittaker, K. W. Lehnert, and R. W. Simmonds, *Nature* **475**, 359 (Jul. 2011)
- [22] F. Massel, T. T. Heikkilä, J. Pirkkalainen, S. U. Cho, H. Saloniemi, P. J. Hakonen, and M. A. Sillanpää, *Nature* **480**, 351 (2011)
- [23] J. D. Teufel, J. W. Harlow, C. A. Regal, and K. W. Lehnert, *Phys. Rev. Lett.* **101**, 197203 (2008)
- [24] T. Rocheleau, T. Ndukum, C. Macklin, J. B. Hertzberg, A. A. Clerk, and K. C. Schwab, *Nature* **463**, 72 (Dec. 2009)
- [25] C. W. Gardiner and M. J. Collett, *Phys. Rev. A* **31**, 3761 (1985)
- [26] Note that tuning the gate voltage also changes the bare frequencies ω_n . What we consider here is the additional frequency shift due to the driving of mode $m \neq n$.
- [27] T. J. Kippenberg, H. Rokhsari, T. Carmon, A. Scherer, and K. J. Vahala, *Phys. Rev. Lett.* **95**, 033901 (2005)
- [28] A. Castellanos-Gomez, H. B. Meerwaldt, W. J. Venstra, H. S. J. van der Zant, and G. A. Steele, *Phys. Rev. B* **86**, 041402 (2012)

APPENDIX : DERIVATION OF THE NON-LINEAR HAMILTONIAN

Expanding u_{ac} in Eq. (2) of the main text on an arbitrary basis $\chi_n(x)$, $u_{ac} = h \sum_n y_n \chi_n$ we get the Hamiltonian of the form

$$H = \frac{p_n^2}{2m} + E_{\text{stress}} \left\{ [\Omega^2]_m^n y_n y^m + \Lambda_{mo}^n y_n y^m y^o + \Theta_{mp}^{no} y_n y^m y_o y^p \right\} + E_g, \quad (15)$$

with the non-linear coefficients

$$[\Omega^2]_m^n = \frac{\omega_0^2}{\omega_s^2} \langle \chi_n'' | \chi_m'' \rangle + \tau \langle \chi_n' | \chi_m' \rangle + 2 \langle \chi_n' | \chi_m' \rangle \langle u'_{dc} | u'_{dc} \rangle + 4 \langle u'_{dc} | \chi_n' \rangle \langle u'_{dc} | \chi_m' \rangle - \frac{V_{dc}^2}{m\omega_s^2 h^2} \int_0^1 \frac{d^2 C[d - u(x, t)]}{du_{dc}^2} \langle \chi_n | \chi_m \rangle dx \quad (16a)$$

$$\Lambda_{mo}^n = 4 \langle u'_{dc} | \chi_o' \rangle \langle \chi_n' | \chi_m' \rangle - \frac{V_{dc}^2}{m\omega_s^2 h^2} \int_0^1 \frac{d^3 C[d - u(x, t)]}{du_{dc}^3} \chi_n \chi_m \chi_o dx \quad (16b)$$

$$\Theta_{mp}^{no} = \langle \chi_n' | \chi_m' \rangle \langle \chi_o' | \chi_p' \rangle - \frac{V_{dc}^2}{m\omega_s^2 h^2} \int_0^1 \frac{d^4 C[d - u(x, t)]}{du_{dc}^4} \chi_n \chi_m \chi_p \chi_o dx \quad (16c)$$

$$E_g = (2V_{dc}V_{ac} + V_{ac}^2) \int_0^1 f(u_o(x)) dx. \quad (16d)$$

Here $C[d]$ is the capacitance between the gate and the beam at the distance d , $\frac{1}{2}m\omega_0^2 h^2 = \frac{EI}{2L^3}$ is the bending energy of a beam displaced by h and $\frac{1}{2}m\omega_s^2 h^2 = \frac{ESh^4}{8L^3}$ is the stress energy of the beam displaced by h with respect to its equilibrium position. The coefficient E_g describes the feedback of the motion of the resonator on the gate voltage and is neglected below as we assume a fixed voltage drive. Besides the voltage, the system is described by the two dimensionless parameters $\tau_0 = 4T_0 L^2 / (ESh^2)$ and $(\omega_0/\omega_s)^2 = 4I_y / (Sh^2)$. For a rectangular beam, which we consider in the following, $(\omega_0/\omega_s)^2 = 1/3$. Overall, our main results do not greatly depend on ω_0 . The thickness h appears in the above expressions only because it sets the magnitude of the deformation — it scales out from the final results of observable quantities.

Writing the Hamiltonian in the basis which diagonalises Ω and scaling hy_n by the amplitude of the zero-point motion $\sqrt{1/m\omega_n}$ one arrives at Eq. (1) of the main text. We consider here specifically a doubly clamped beam. For low voltage the DC deformation u_{dc} is given by the Euler–Bernoulli equation in the case of a parallel plate capacitance model:

$$m\omega_0^2 h u_{dc}'''' - \left(m\omega_T^2 h + 2m\omega_s^2 h \int_0^1 u_{dc}^2 dx \right) u_{dc}'' = \frac{V_g^2}{2} \frac{\epsilon WL}{d^2}. \quad (17)$$

The solution of this integro-differential equation is [11]

$$u_{dc} = \frac{\tilde{V}^2}{8\tau\xi} \left(\coth\left(\frac{\xi}{2}\right) (\cosh(\xi x) - 1) - \sinh(\xi x) + \xi x - \xi x^2 \right), \quad (18)$$

where $\tilde{V}^2 = (-h\partial_d C V_g^2) / E_{\text{stress}}$, $E_{\text{stress}} = m\omega_s^2 h^2 / 2 = ESh^4 / (8L^3)$. We define the total tension

$$\tau = \tau_0 + 2 \int_0^1 u_{dc}^2 dx \quad (19)$$

and $\xi = \sqrt{3\tau}$. Substituting Eq. (18) into Eq. (19), integrating and then disregarding exponential terms $\sim \exp(-\xi)$ yields a self-consistency equation for τ ,

$$\tau = \tau_0 + \frac{\tilde{V}^4}{96\tau^2} \left(1 - \frac{3\sqrt{3}}{\sqrt{\tau}} + \frac{8}{\tau} \right), \quad (20)$$

Since in the limit of large τ Eq. (17) reduces to the wave equation, we use the harmonic wave function $\chi_n =$

$\sqrt{2}\sin(n\pi x)$ as a basis for (17) and get

$$[\Omega^2]_m^n = \frac{(n\pi)^4}{3} + \tau(n\pi)^2 + \frac{\tilde{V}^4}{8\tau^2} f_n(\tau) f_m(\tau) - \frac{\tilde{V}^2}{2} \frac{h}{d} \quad (21a)$$

$$\Lambda_{mo}^n = \sqrt{2}(n\pi)^2 \frac{\tilde{V}^2}{2\tau} f_o(\tau) \delta_m^n - \frac{\tilde{V}^2}{2} \left(\frac{h}{d}\right)^2 \frac{4\sqrt{2}mno((-1)^{m+n+o}-1)}{\pi(m-n-o)(m+n-o)(m-n+o)(m+n+o)} \quad (21b)$$

$$\Theta_{mp}^{no} = (n\pi)^2 (p\pi)^2 \delta_m^n \delta_p^o - \frac{\tilde{V}^2}{2} \left(\frac{h}{d}\right)^3 \frac{1}{2} [\delta_{n+m+o,-p} + \delta_{n+m,o+p} + \delta_{n+p,m+o} + \delta_{n+o,m+p} - \delta_{n+m+o,p} - \delta_{n+m+p,o} - \delta_{n+o+p,m} - \delta_{m+o+p,n}] \quad (21c)$$

$$f_n(\tau) = n\pi(1 - (-1)^n) \left(\frac{2}{\pi^2 n^2} - \frac{\sqrt{3}\tau}{\pi^2 n^2 + 3\tau} \right). \quad (21d)$$

The last terms in Eqs. (21a), (21b) and (21c) are relevant only for low voltages in the presence of initial tension, and do not greatly contribute to the physics discussed in this paper. We thus drop them out in the ensuing analytical approximations. However in the numerical results, we use the full solutions of the Euler–Bernoulli equation to determine the eigenmodes and the coupling constants. Nevertheless, Eqs. (21a-21c) represent a fairly approximations in the limit of relatively strong tension.

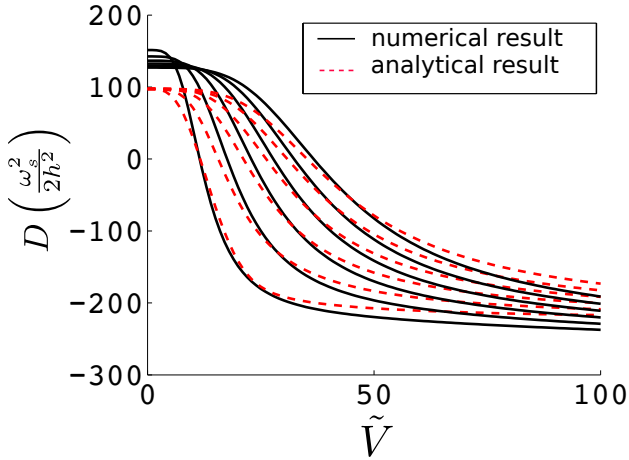


FIG. 4. Duffing constant for the first mode with different initial tension τ . From left to right the dimensionless initial tension τ_0 starts from 0 and increases with the step of 10. The dashed lines are our analytic expressions and the full line are numerical solutions of the full Euler–Bernoulli equations obtained from Eq. (2) of the main text. The deviation between the two set of curves at low V is due to our scheme of approximating mode functions by harmonic functions.

DUFFING CONSTANT

We can estimate the overall behavior of the Duffing constant $D = \omega_s^2/(2h^2) [(\Theta_{nn}^{nn})_d - \frac{5}{4}(\Lambda_{nn}^n)_d^2/[2(\Omega_n^n)_d^2]]$ by

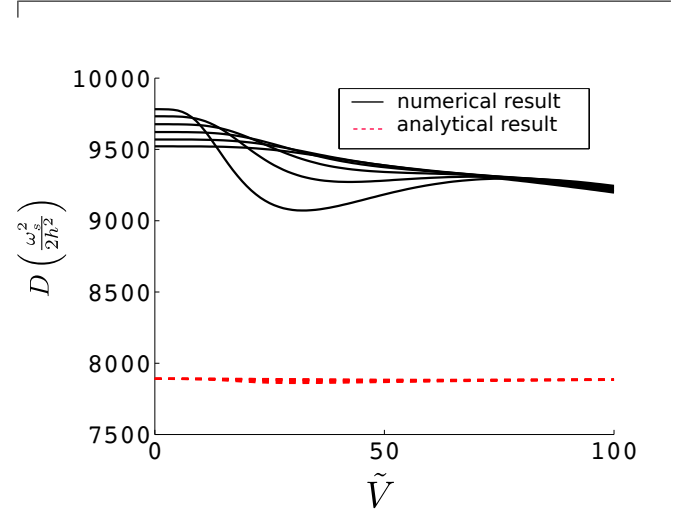


FIG. 5. Duffing constant for the third mode with different initial tensions τ_0 . From left to right the dimensionless initial tension τ_0 starts from 0 and increases with the step of 10. The dashed lines are our analytic expressions and the full line are numerical solutions of the full Euler–Bernoulli equations obtained from Eq. (2) of the main text. The approximation with harmonic mode functions underestimates Θ_{mp}^{no} , which is the reason for the discrepancy between the full numerical solutions and our analytic approximations.

disregarding the off-diagonal terms in Eqs. (21a-21b) and solving the tension τ with Eq. (20). The tension τ exhibits a rather complicated voltage dependence, however its behaviour can be investigated in different limiting cases. A characteristic value for the voltage can be found by substituting $\tau \equiv \tau_0$ into Eq. (20) and comparing τ_0 to the second terms of the right hand side of Eq. (20). This yields

$$\tilde{V}^* = 96^{1/4} \frac{\tau_0^{3/4}}{\left(1 - 3\frac{\sqrt{3}}{\sqrt{\tau_0}} + \frac{8}{\tau_0}\right)^{1/4}}. \quad (22)$$

Thus we find that for $\tilde{V} \ll \tilde{V}^*$ the tension $\tau \approx \tau_0$ while for $\tilde{V} \gg \tilde{V}^*$ we have $\tau \approx \frac{V^{4/3}}{96^{1/3}}$. Disregarding terms coming from the electrostatic force the general expression

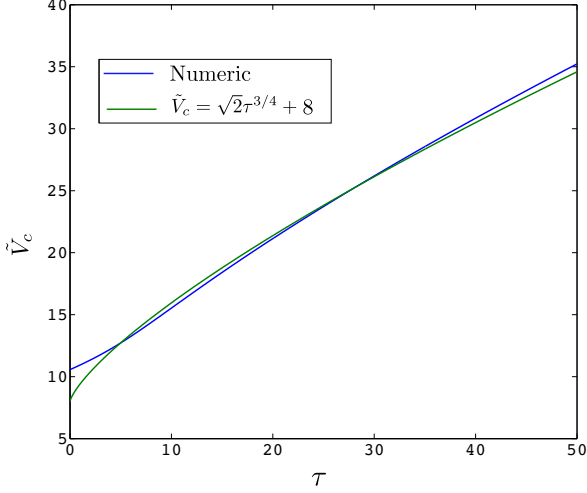


FIG. 6. Crossover voltage V_c for the sign change of the Duffing constant with respect to the initial tension τ .

for the Duffing constant is

$$D = \frac{\omega_s^2}{2h^2} \left[(n\pi)^4 - \frac{5}{8} \frac{(n\pi)^4 f_n(\tau)^2 \frac{V^4}{\tau^2}}{\frac{4I_y(n\pi)^4}{Sh^2} + \tau(n\pi)^2 + f_n(\tau)^2 \frac{V^4}{8\tau^2}} \right]. \quad (23)$$

As shown in Figs. 4, 5, at low \tilde{V} , D starts from a positive value $D(V=0) \approx \omega_s^2/(2h)^2(n\pi)^4$ and tends to a voltage-independent value $D(\tilde{V}) = \omega_s^2/(2h^2) \left[\frac{(n\pi)^4[(n\pi)^4 - 768]}{192 + (n\pi)^4} \right]$ at large voltages. Note that, for a symmetric dc deformation, this behavior is only valid for odd-order modes (with symmetric eigenfunctions with respect to the center of the beam). Indeed, from Eq. (21d), we find that the Duffing constant is voltage independent for an even n . In Fig. 4, we plot the behaviour of the Duffing constant for the first mode for different values of τ . We find that D changes its sign for a given value of the voltage, $\tilde{V} = \tilde{V}_c$ and the effect of the initial tension is to shift the crossover voltage to higher values (Fig. 6). For $n > 1$ the Duffing constant varies only weakly with \tilde{V} and stays always positive (see Fig. 5).

MODE COUPLING

The frequency response function f for the input signal δa_n^{in} solved from Eqs. (10-11) of the main text is

$$f = -i\sqrt{\gamma_n} \frac{\left[\Delta^2 + \left(\frac{\gamma_m}{2} - i\omega \right)^2 - c^2 |\alpha_m|^4 \right] \left[a + i\frac{\gamma_n}{2} + \omega + \omega_n \right] - 2b^2 |\alpha_m|^2 (\Delta + c|\alpha_m|^2)}{\left[\Delta^2 + \left(\frac{\gamma_m}{2} - i\omega \right)^2 - c^2 |\alpha_m|^4 \right] \left[\left(\frac{\gamma_n}{2} - i\omega \right)^2 + \omega_n^2 + 2a\omega_n \right] - 4\omega_1 b^2 |\alpha_m|^2 (\Delta + c|\alpha_m|^2)} \quad (24)$$

with

$$\begin{aligned} a &= 12F_n(\alpha_n + \alpha_n^*)^2 + 6T_n(\alpha_n + \alpha_n^*) + 4F_{nnmm}|\alpha_m|^2 + 2F_{nnmm} \\ b &= 4F_{nnmm}(\alpha_n + \alpha_n^*) + 2T_{nnmm} \\ c &= 12F_m. \end{aligned}$$

This frequency response function describes a Lorentzian resonance around an effective frequency $\omega_{n,\text{eff}}$ with damping $\gamma_{n,\text{eff}}$ described in Eqs. (12) and (13) of the main text. Using the approximations leading to Eqs. (16) we find the effective frequency

$$\begin{aligned} \frac{\omega_{n,\text{eff}} - \omega_n}{\chi} &= n^2 m^2 \pi^4 \left[8 - \frac{3f_n(\tau)^2 \frac{\tilde{V}^4}{\tau^2}}{\frac{4I_y(n\pi)^4}{Sh^2} + \tau(n\pi)^2 + f_n(\tau)^2 \frac{\tilde{V}^4}{8\tau^2}} \right. \\ &\quad \left. \mp \frac{m^2}{4n^2} \frac{f_n(\tau)^2 \frac{\tilde{V}^4}{\tau^2}}{\sqrt{\left(\frac{4I_y(n\pi)^4}{Sh^2} + \tau(n\pi)^2 + f_n(\tau)^2 \frac{\tilde{V}^4}{8\tau^2} \right) \left(\frac{4I_y(m\pi)^4}{Sh^2} + \tau(m\pi)^2 + f_m(\tau)^2 \frac{\tilde{V}^4}{8\tau^2} \right)}} \right] \end{aligned}$$

and effective damping

$$\frac{\gamma_{n,\text{eff}} - \gamma_n}{\chi Q_m} = \pm \frac{2(m\pi)^4 f_n(\tau)^2 \frac{\tilde{V}^4}{4\tau^2}}{\frac{4I_y(m\pi)^4}{Sh^2} + \tau(m\pi)^2 + f_m(\tau)^2 \frac{\tilde{V}^4}{8\tau^2}}. \quad (25)$$

Here $\chi = 4m\omega_s^2 |\alpha_m|^2 x_{z_{pm}}^2 \frac{x_{z_{pn}}^2}{fh^2}$ describes the amplitude of the pump.

In Fig. 3 of the main text, we plot the effective frequency and the effective damping when driving mode $m = 3$ and probing its effect on mode $n = 1$. We see that, for red-detuned pumping with $\Delta = \omega_n$, the frequency shift induced by pumping is positive at low gate voltages, $\omega_{n,\text{eff}}(V_g = 0) - \omega_n = (n\pi)^2(m\pi)^2\chi$, changes sign with increasing dc gate voltage, and tends to a voltage-independent value at large voltages

$$\omega_{n,\text{eff}} - \omega_n \xrightarrow{\tilde{V} \gg \tau_0, 1} \chi(nm)^2 \pi^4 \left[8 - \frac{4608/(n\pi)^2}{(n\pi)^2 + 192/(n\pi^2)} - \frac{m^2}{n^2} \frac{384/(n\pi)^2}{\sqrt{[(n\pi)^2 + 192/(n\pi^2)][(m\pi)^2 + 192/(m\pi^2)]}} \right]. \quad (26)$$

On the other hand the effective damping increases with an increasing gate voltage until it reaches a voltage-independent value

$$\frac{\gamma_{n,\text{eff}} - \gamma}{\chi Q_m} = \frac{m^6}{n^4} \frac{768\pi^4}{\pi^4 m^4 + 192}. \quad (27)$$

For blue-detuned driving, when $\Delta = -\omega_n$, the optical spring effect ($\omega_{n,\text{eff}} - \omega$) increases until it saturates at large voltages to the value

$$\omega_{n,\text{eff}} - \omega_n \xrightarrow{\tilde{V} \gg \tau_0, 1} \chi(nm)^2 \pi^4 \left[8 - \frac{4608/(n\pi)^2}{(n\pi)^2 + 192/(n\pi^2)} + \frac{m^2}{n^2} \frac{384/(n\pi)^2}{\sqrt{[(n\pi)^2 + 192/(n\pi^2)][(m\pi)^2 + 192/(m\pi^2)]}} \right] \quad (28)$$

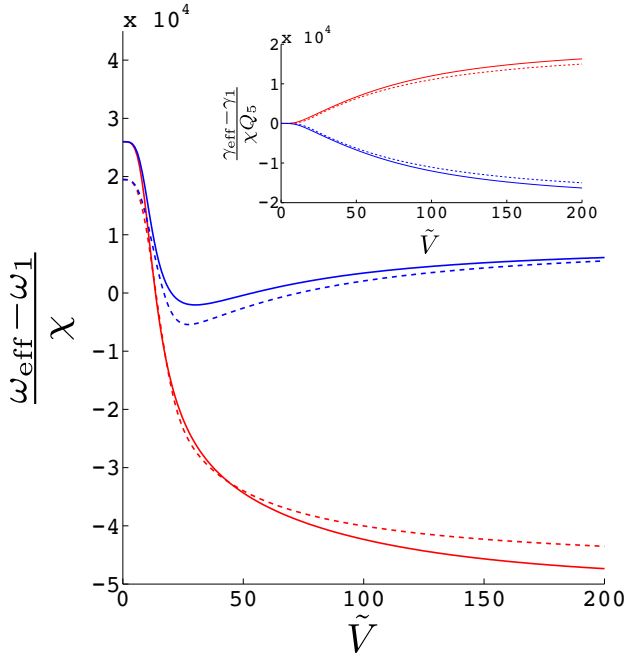


FIG. 7. Effective frequency and damping (inset) of mode $n = 1$ when driving mode $m = 5$ and when initial tension $\tau_0 = 0$ in the case of red detuning (red lines, lower) with $\Delta = \omega_1$ and in the case of blue detuning (blue lines, upper) with $\Delta = -\omega_1$. The full lines are numerical results obtained by solving the full Euler–Bernoulli equation and dashed lines are analytical results derived in the text.

while the damping decreases until it reaches the value

$$\frac{\gamma_{n,\text{eff}} - \gamma}{\chi Q_m} = -\frac{m^6}{n^4} \frac{768\pi^4}{\pi^4 m^4 + 192} \quad (29)$$

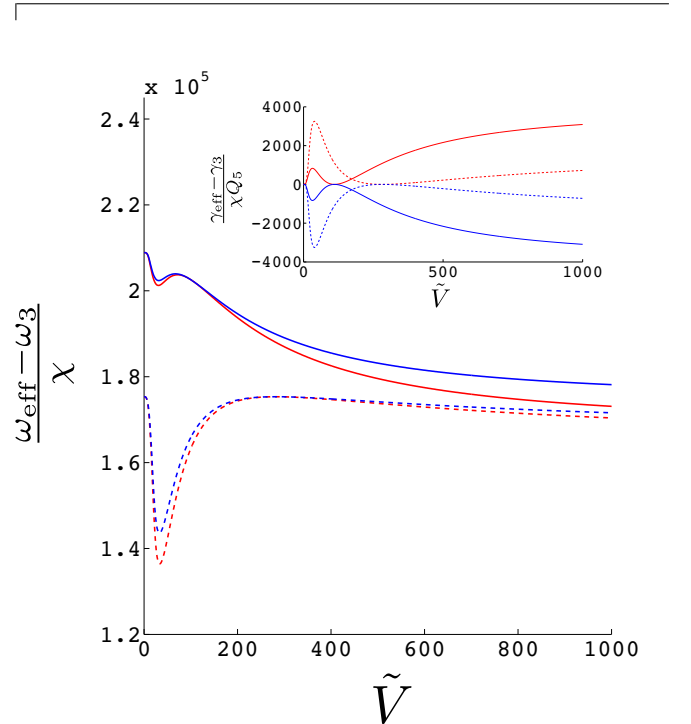


FIG. 8. Effective frequency and damping (inset) of mode $n = 3$ when driving mode $m = 5$ and when initial tension $\tau_0 = 0$ in the case of red detuning (red lines, lower) with $\Delta = \omega_3$ and in the case of blue detuning (blue lines, upper) with $\Delta = -\omega_3$. The full lines are numerical results obtained by solving the full Euler–Bernoulli equation and dashed lines are analytical results derived in the text.

These predictions are compared to the full numerical solutions obtained from the Hamiltonian Eq. (2) of the main text in Fig. 3 of the main text. Although we are focusing only on the first and third mode in the main

text one can also consider pairs of other modes. We plot the effective frequency and effective damping for $n = 1$ and $m = 5$ in Fig. 7 and for $n = 3$ and $m = 5$ in Fig. 8. In the first case when driving mode $m = 5$ and measuring mode $n = 1$ the change in the effective frequency is larger than the one we have when driving mode $m = 3$. We also find that in the case of blue detuning the effec-

tive frequency changes its sign twice as a function of the gate voltage. When driving mode $m = 5$ and measuring mode $n = 3$, the voltage dependence of the change in the effective frequency is relatively small as the fourth-order term dominates throughout the interesting regime of voltages.